Title: Variation in relaxation of non-photochemical quenching between the founder genotypes of the soybean (Glycine max) nested association mapping population

Dhananjay Gotarkar[1,2] (0000-0002-6577-9954)
Anthony Digrado[1,3] (0000-0002-8624-9290), adigrado@illinois.edu
Yu Wang[1] (0000-0002-6951-2835), yuwangcn@illinois.edu
Lynn Doran[1] (0000-0001-6358-8524), ldoran@illinois.edu
Bethany Blakey[3] (0000-0001-9923-0794), blakely6@illinois.edu
Brian W. Diers[4] (0000-0003-3584-5495), bdiers@illinois.edu
Daniel J. Eck[5] (0000-0002-2571-5331), dje13@illinois.edu
Steven J. Burgess[1,2*] (0000-0003-2353-7794), sjb287@illinois.edu

[1] Carl R Woese Institute for Genomic Biology, University of Illinois Urbana-Champaign, Urbana, IL, USA
[2] Department of Plant Biology, University of Illinois Urbana-Champaign, Urbana, IL, USA.
[3] Global Change and Photosynthesis Research Unit USDA ARS, Urbana, IL, USA.
[4] Department of Crop Sciences, University of Illinois Urbana-Champaign, Urbana, IL, USA.
[5] Department of Statistics, University of Illinois Urbana-Champaign, Urbana, IL, USA.

*Corresponding author
Full address: 283 Morrill Hall, 505 S. Goodwin Avenue, University of Illinois Urbana-Champaign, Urbana IL 61801, USA
E-mail address: sjb287@illinois.edu
Phone number: +1 217-244-8179

Keywords

Non-photochemical quenching, photosynthesis, Glycine max

Summary

Improving the efficiency of crop photosynthesis has the potential to increase yields. Genetic manipulation showed photosynthesis can be improved by speeding up relaxation of photoprotective mechanisms during sun to shade transitions. However, it is unclear if natural variation in relaxation of non-photochemical quenching (NPQ) can be exploited in crop breeding programs. To address this issue, we measured six NPQ parameters in the 40 founder lines and common parent of a Soybean Nested Association Mapping (SoyNAM) panel over two field seasons in Illinois. NPQ parameters did not show consistently variable trends throughout development, and variation between sampling days suggests environmental impacts on NPQ which last more than 24 hours. 17 genotypes were found to show small but consistent differences in NPQ relaxation kinetics relative to a reference line providing a basis for future mapping studies. Finally, a soybean canopy model predicted available phenotypic variation could result in a 1.6% difference in carbon assimilation when comparing fastest and slowest relaxing NPQ values.

Significance Statement

Evidence suggests increasing the rate of relaxation of photoprotection can lead to improved biomass and yield. We compare photoprotection relaxation rates in 41 diverse soybean genotypes grown in the field, identifying lines with faster rates of relaxation, and predict a potential 1.6% difference in daily carbon assimilation which could contribute to improving soybean performance.

Introduction

Leaves within a canopy are exposed to sunflecks and shadeflecks, caused by intermittent cloud cover, wind induced leaf movements, and the changing angle of the sun (Kaiser *et al.*, 2018). Balancing variable energy supply with demand for reducing equivalents is essential for efficient photosynthesis (Kramer and Evans, 2011) and a delay in adjustment of biochemical or gas diffusional processes can lead to reduced carbon assimilation (Sakoda *et al.*, 2022).

In response to excess light, plants activate photoprotective mechanisms (Demmig-Adams *et al.*, 2012; Jahns and Holzwarth, 2012) which deal with production of reactive oxygen species and limit photoinhibition (Pinnola and Bassi, 2018). Excess absorbed light energy can be dissipated by non-photochemical quenching (NPQ) of chlorophyll excited states, reducing the likelihood that damaging reactive oxygen species are formed (Patricia Müller *et al.*, 2001; Ruban and Wilson, 2021). Transgenic approaches have shown increasing NPQ in rice can lead to increased biomass production in glasshouse conditions by alleviating photoinhibition (Hubbart *et al.*, 2018). However, excess NPQ, or delays in relaxing NPQ during shadeflecks, are predicted to cause unnecessary dissipation of energy, reducing the efficiency of photosynthesis (Zhu *et al.*, 2004; Burgess *et al.*, 2019). As a result, speeding up NPQ activation and relaxation can improve photosynthetic efficiency (Kromdijk et al., 2016; Garcia-Molina and Leister, 2020; De Souza et al., 2022; Lehretz et al., 2022). Support for a link between fast relaxation of NPQ and increased biomass accumulation comes from African rice genotypes grown under controlled conditions (Cowling *et al.*, 2022). Further, analysis of transgenic plants in small-scale field experiments suggested an increase biomass in Tobacco (Kromdijk *et al.*, 2016) and seed production in soybean (De Souza *et al.*, 2022) could be achieved if NPQ relaxation is accelerated. However, there have been contrasting results in Arabidopsis (Garcia-Molina and Leister, 2020) and potato (Lehretz *et al.*, 2022), while the manipulating NPQ on soybean seed production differed between years (De Souza *et al.*, 2022). Taken together, these data point to the need to further understand species the relation of photoprotection to whole plant physiology if the potential benefits of altering NPQ are to be translated to commercial crop varieties (Kaiser *et al.*, 2019; Leister, 2023).

Most experiments investigating NPQ have been performed under controlled conditions or at a single time point during development. However, NPQ is highly dynamic and sensitive to any perturbation which impacts carbon assimilation or cellular redox state. This means in a field environment, NPQ is likely to vary in response to weather conditions (Zhu *et al.*, 2009; Porcar-

Castell, 2011; Sun *et al.*, 2020), but the relationship between genotype x environment interactions on NPQ kinetics is poorly understood. Two studies with field grown soybean have assessed photosynthetic parameters with analysis of chlorophyll fluorescence, using canopy reflectance to calculate photochemical reflectance index (PRI) as a proxy for NPQ (Herritt *et al.*, 2016), and OJIP transients to look at variation in fluorescence kinetics (Herritt *et al.*, 2018). However, the individual components of NPQ relaxation were not assessed. Therefore, the extent to which individual components of NPQ co-vary in natural populations and whether they can be selected in breeding programs remains unclear.

A nested association mapping panel has been developed for soybean with the aim of identifying beneficial alleles possessed by elite and exotic germplasm (SoyNAM)(Song *et al.*, 2017; Diers *et al.*, 2018). This population has proved useful for studying agronomic traits and how they impact yield (Song *et al.*, 2017; Diers *et al.*, 2018; Lopez *et al.*, 2019; Montes *et al.*, 2022). We sought to use this resource for analysis of NPQ relaxation, and kinetics were measured for the 41 SoyNAM founder lines over the course of a field season in 2021 and 2022. The goals of this study were to (1) assess if NPQ kinetics vary in response to developmental and field environmental conditions, (2) identify soybean genotypes with fast relaxation kinetics that could serve as the basis for genetic mapping, and (3) test the impact of altering NPQ relaxation on carbon assimilation using a soybean canopy model given existing diversity.

Six parameters were calculated by fitting a double exponential function to the decay in NPQ on transition to low light (Dall'Osto *et al.*, 2014), including fast (qE) (Krause *et al.*, 1982) and intermediate (qM) relaxing NPQ and their respective rate constants (τ_{qE} and τ_{qM}), in addition to long term NPQ (qI) and maximum NPQ reached during high light treatment (Table 1). Repeat measurements were taken throughout the growing season and a mixed effects linear modeling approach was used to identify lines with significantly different values for NPQ relaxation. Finally, a canopy photosynthesis model (Wang *et al.*, 2020) was used to estimate the potential impact of genetic improvement in NPQ relaxation on soybean photosynthesis.

Results

Measurements of NPQ relaxation in field grown plants were taken between V1 to R6 maturity stages in 2021 and 2022 (Figure 1, Table S1-2). Although NPQ parameters remained largely consistent over the course of the growing season, some days exhibited variations in mean values and variance. For instance, declines in τ_{qE} and A_{qM} were observed on the fourth and fifth sampling days in 2022 (Figure 1a and b).

Variation in NPQ relaxation parameters. For all parameters measured there were significant differences between genotypes (G) and days (E) (Table 2). This indicated significant differences between genotypes and a strong impact of the environment on NPQ relaxation. However, there was no significant G x E interaction, suggesting genotypes responded similarly to the environment (Table 2). A stepwise AIC-based model revealed that the environment explained 10-47% of the observed variance in NPQ relaxation depending on the parameter and year (Figure 2). The parameter Aq_l was the best explained by the environment, with a R^2>0.3 in both years. The parameter τ_{qM} remained the parameter for which the environment had the least predictive power, with a R^2<0.16 for both years. The R^2 for the other parameters varied between years with, for instance, τ_{qE} showing a R^2 of 0.08 in 2021 and 0.32 in 2022. This could be explained by the range of variation observed in these parameters during those years. For both 2021 and 2022, the high values for the Precip and F_{sd} coefficients indicate their strong impact on the parameters, followed by VPD. The years 2021 and 2022 distinguished themselves as VPD_7day had a stronger impact in 2021 compared to 2022 where VPD was preferred by the model. The variable Ta_7day had a significant impact on the NPQ parameters in 2022. Between years, the parameters were affected differently by their environment, with A_{ql} being affected positively by Ta_7day, Precip, and F_{sd} in 2021, but showing the opposite behavior in 2022. This might be due different environmental patterns between the two years, with 2022 showing higher VPD and lower precipitation at the beginning of the growing season compared to 2021. However, A_{qE}, τ_{qE}, and maxNPQ were affected in the same manner by the environment. When the two years were combined in a single model, Precip_7day, Precip_cum, Fsd_7day, and cumFn were included in the final models (Figure S1). Their absence in the 2021 and 2022 models suggest these variables mostly contributed to explain the year to year variation in NPQ relaxation parameters.

Canonical correlation analysis (CCA) was used to further explore the relationship between NPQ relaxation parameters and the environment within the NAM founders. The canonical correlations

between pairs were ≥0.4 (p-value<0.001, Table 3), allowing association of changes in the environment with changes in NPQ relaxation. For both years, CCA revealed seasonal patterns in the NPQ relaxation parameters (Figure 3). In 2021, the CCA showed a change in environmental conditions throughout the season, with an increase in VPD, Ta, F_{sd}, cumFn, and a decrease in precipitation between June 24th and July 20th (Figure 3b, d). This was associated with an increase in A_{ql} and a decline in A_{qE} (Figure 3a, c). The NPQ parameter τ_{qE} remained constant. This is in accordance with the stepwise regression analysis which showed a low predictive power of environmental variable on τ_{qE} in 2021 (Figure 2). Past July 20th, the environmental conditions showed less variation. This was associated with less fluctuation in the different NPQ parameters. July 7th distinguished itself from the other days by an increase in A_{qM}, maxNPQ, and τ_{qM}. In 2022, the CCA showed a somewhat similar pattern with an increase in A_{ql} at the beginning of the growing season (from July 6th to July 26th) but accompanied by a decline in A_{qM} (Figure 3e, g). This was associated with lower Ta, VPD, and F_{sd} over the same period (Figure 3f, h). The transition from August to July was marked by increasing precipitation and a decline in Ta_7day. This was associated with increasing maxNPQ and a decline in τ_{qM}. Between August 4th and August 20th, the opposite behavior was observed with an increase in A_{qM} and a decline in A_{ql}. Overall, both years showed an increase in A_{ql} at the beginning of the season and highlighted a seasonal behavior with a period of important changes in NPQ relaxation associated with changes in environmental conditions. CCA also revealed different behavior in some NPQ relaxation parameters between years, with τ_{qE} showing no variations in response to its environment in 2021 but being positively associated with Ta_7day, VPD, and cumFn in 2022. The CCA revealed no striking differences between the different NAM groups as they showed the same seasonal behavior in both years, which suggest a stronger impact of the environment on NPQ relaxation than a genotypic variation over the season.

Variation in NPQ parameters between NAM founders. To identify any variation between the NAM founders within a day, a Principal Components Analysis (PCA) was run for each day (Figure S2-14). The Diverse, Elite, PI, and RC groups are highlighted. The results showed no distinction between those groups, which tended to overlap (Figure S2-14). To determine if the groups were significantly distinct from each other, a linear model followed by an ANOVA was used on the principal component coordinate with the 'NAM groups' set as a fixed factor. This analysis showed some significant differences between groups on some dates (Table 4). Groups clusters also separated between group on 6/24/21 and 8/4/22 on the PC2. Groups also separated on the PC3 on 7/13/21 (Figure S5) and 7/6/22 (Figure S9). This suggest that some

groups distinguished themselves from the others on the parameters that were the most strongly correlated with these axes. For instance, on 8/4/22 (Figure S13), groups separated on the second component, with PIs showing higher values in A_{qE} and maximum NPQ on average (Figure S13). Founders of NAM10, NAM31, and NAM33 detached themselves from the population cluster on two or more occasions. For instance, on those occasions, NAM33 founder tended to locate in region of the PCA associated with higher maximum NPQ on 6/24/21 (Figure S2) and 7/28/21 (Figure S7).

When considering all days combined the largest range in values between genotypes was seen in mean τ_{qM} values, which varied ~1.5 fold between the founder genotypes of NAM5 (19.94) and NAM17 (29.3) (Figure 4; Table 5; Table S3). A small range of values was observed for all other parameters (Table 2; Figure 4) and no observable difference was seen between elite, diverse or PI genotypes (Figure 4) consistent with the PCA (Figure S2-15). A mixed effects linear model was employed to test whether genotypes showed consistent variation relative to the reference genotype RC, while considering development stages and environmental conditions on NPQ relaxation parameters. Nested model comparisons via AIC indicated 17 genotypes varied consistently in at least one parameter over six different models compared to RC (Figure 5). Three genotypes consistently varied in two parameters, with founders of NAM33 and 37 having lower A_{qI} and MaxNPQ compared to RC, while the NAM54 founder had slower relaxation of A_{qM} represented by a larger τ_{qM}, and a higher maximum NPQ (Figure 5).

Modeling impact of NPQ variation on canopy photosynthesis. To assess the potential for improving the efficiency of soybean photosynthesis a canopy model, parameterized for reference line RC was used to calculate the impact of varying NPQ parameters based on the phenotypic diversity present in the SoyNAM founders. The minimum and maximum recorded genotypic values for NPQ relaxation (τ_{qE} and τ_{qM}) were used to estimate the potential decrease in CO_2 assimilation caused by slow relaxation of NPQ on a cloudy (226) and sunny (227) day in Illinois in 2021 (Figure 6a and b). Simulations estimate the difference in CO_2 assimilation between canopies with the fastest and slowest relaxing NPQ kinetics observed would equate to 1.6% on intermittently cloudy days, and 1.1% on a sunny day (Figure 6c).

Discussion

The aims of this study included assessing the extent of variation in NPQ relaxation parameters between SoyNAM founder genotypes and predicting the impact on canopy photosynthesis. Given that we identified strong environmental effects on measured NPQ parameters, (Figure 2-3, Figure S1), our data are consistent with differences caused by physiological adaptation that lasts longer than 24h. This was brought to light by Figure S1, highlighting the importance of 7 day-averaged variables to explain the variation between years that daily averages couldn't explain. The mechanisms behind this phenomenon are unclear, but it is possible that the phenotype is influenced by the status of xanthophyll cycle pigments in the leaf. Zeaxanthin (Zx), plays an important role in modulating NPQ and is created from the de-epoxidation of violaxanthin (Vx) via the intermediate antheraxanthin (Ax) (Jahns and Holzwarth, 2012). Zx decelerates the relaxation of qE (Niyogi *et al.*, 1998) and the rate of conversion to Vx appears to be indirectly associated with slower relaxing phases of NPQ referred to as qZ (Nilkens *et al.*, 2010; Kress and Jahns, 2017). The amount is Zx is dependent on the combined xanthophyll pool size (VAZ), which is regulated by carotene hydroxylase (Davison *et al.*, 2002), and the steady state de-epoxidation state of xanthophyll pigments which is influenced by the activity of zeaxanthin epoxidase (ZEP). The VAZ pool size is adjusted in response to environmental conditions, with studies showing that leaves grown in full sun as opposed to shade conditions have larger pools (Demmig-Adams, 1998), with a greater de-epoxidation state, and more Zx would be expected to lead to an increase in τ_{qE}. However, there is currently a limited understanding of regulation of xanthophyll cycle enzymes in response to environmental stress, which appears to vary between tissues, species and cultivars (Schwarz *et al.*, 2015; Bethmann *et al.*, 2019; Grieco *et al.*, 2020). For example, ZEP degraded in leaves but accumulated in roots of Arabidopsis exposed to drought stress (Schwarz *et al.*, 2015). Whereas ZEP was shown to increase in abundance of leaves from an Iranian cultivar of wheat exposed to a water stress, but not one from the UK, while violaxanthin de-epoxidase (VDE) remained stable (Grieco *et al.*, 2020). Interestingly, the wheat plants with increased ZEP were characterized by a higher qZ amplitude (Zx-dependent quenching on 10-30 min time scale) and a higher τ_{qZ} relative to control as the drought treatment established, which would have been expected if VDE had increased or ZEP decreased. This has led the authors to hypothesize that the slowdown in NPQ was caused by a change in enzyme activity rather than in stoichiometry (Grieco *et al.*, 2020). While it is difficult to determine whether the soybeans have been experiencing water stress during our study, the decline in τ_{qM} (which would be the parameter the most related to τ_{qZ}) in 2022 coincided with precipitation events that had followed a sustained period with low precipitations

(Figure 2) which would be consistent with increased ZEP activity. However, further investigation is required to determine if xanthophyll pigment content and enzyme abundance can account for the observed impact of other environmental variables on NPQ relaxation.

Fast conformational change in the thylakoid membrane is also known to play an important role in NPQ and its components (Schaller *et al.*, 2010; Ruban *et al.*, 2012; Sacharz *et al.*, 2017). PsbS has been proposed to facilitate thylakoid membrane re-organization by regulating the interaction between LHCII and PSII which then results in NPQ (Kiss *et al.*, 2008). A study conducted on a PsbS knock-out rice mutant revealed that τ_{qE} depended on the level of phosphorylation of Lhcb1 and Lhcb2 (Pashayeva *et al.*, 2021). High temperature has been shown to lead to an increase in the thylakoid membrane stiffness, causing a decline in the amplitude of the long-lifetime components of fluorescence decay without affecting its lifetime (Pollastri *et al.*, 2019). While it difficult in our study to isolate the effect of air temperature on NPQ relaxation from the effect of other environmental variables, our results showed an important impact of temperature on NPQ relaxation and its varied components (Figure 2, Figure S1), though its effect varied depending on the year and the components. How multiple environmental stressors may interact and affect NPQ relaxation remains understudied.

Our study also revealed a seasonal pattern in NPQ relaxation (Figure 3) and the importance of aggregated environmental variables (Figure S1) when comparing NPQ relaxation between years, suggesting a lasting effect of the environment on NPQ relaxation. Photoinhibitory quenching has been shown to operate at a seasonal timescale (Demmig-Adams and Adams III, 2006) and could have a lasting impact on NPQ relaxation. Long-term adaptation of NPQ has been observed in *Taxus baccata* with needles exposed to high light in winter showing a slowed NPQ relaxation weeks after (Robakowski and Wyka, 2009). Studies have also shown that repeated excess-light exposure can lead to a faster onset kinetics of pH-dependent NPQ (Demmig-Adams *et al.*, 2022). This was true for both sun-grown and shade leaves. Still, more studies are needed to understand how NPQ relaxation is affected by its environment on a longer timescale in crops.

The SoyNAM population is known to possess genotypic diversity with respect to photosynthetic variables: there is large variation in rates of rubisco activation, which was reported to cause a >5 fold difference in carbon fixation during the first five minutes following transition between dark and light conditions (Soleh *et al.*, 2017), and loci have been identified influencing carbon

assimilation and electron transport (Montes *et al.*, 2022). Intriguingly the founder genotype of NAM12, which has previously been shown to possess highest levels of steady state electron transport (J_{max}) (Montes *et al.*, 2022), and slowest rate of rubisco activation (Soleh *et al.*, 2017), was the only genotype that showed significantly slower rates of relaxation of qE relative to the reference (Figure 4). But further analysis of RIL population will be required to determine if these traits are linked or segregate independently. A known variant is found at the *e2* locus, which encodes homolog of the Arabidopsis circadian clock gene GIGANTEA (Watanabe *et al.*, 2011). This gene have been shown to have pleiotropic effects which influence soybean photosynthesis (Montes *et al.*, 2022), canopy coverage (Xavier *et al.*, 2017) and yield traits (Diers *et al.*, 2018). The late maturity *E2* allele is segregating in seven of the NAM founders, three of which (NAM33, 37 and 50) were identified as having significantly less A_{ql} compared to the reference line, and it may therefore also influence the traits measured here.

Although a small number of lines were found to vary in NPQ kinetics compared to RC (Figure 4), the overall diversity in NPQ relaxation parameters between SoyNAM founders was limited, for example, only a 1.5-fold change between the smallest and highest τ_{qM} (Table 5). This small amount of variation is not a general phenomenon related to NPQ, with several studies finding substantial variation in species ranging from Arabidopsis to Maize (Jung and Niyogi, 2009; Rungrat *et al.*, 2019; Cowling *et al.*, 2022; Sahay *et al.*, 2023). For example, analysis of rice genotypes found large variation maximum NPQ (Kasajima *et al.*, 2011), which was attributed to an insertion in the promoter region of photosystem II subunit S (PsbS) resulting in higher expression and higher NPQ in japonica rice (Wang *et al.*, 2017). In the case of soybean, this lack of variation may reflect an unusual number of genetic bottlenecks in domestication and then introduction into the USA (Hyten *et al.*, 2006), with only 28 ancestors contributing to 95% of the genes in cultivars released between 1947-1988 (Gizlice *et al.*, 1994). The lines used in this study were chosen for their diversity, but it remains unclear if there is more variation in NPQ to be found in the wider soybean germplasm and whether more may be found in collections of the wild ancestor *Glycine soja* which is considered a largely untapped source of genetic variation in cultivated soybean (Kofsky *et al.*, 2018).

Previous transgenic manipulations suggested that speeding up relaxation of NPQ can increase photosynthetic efficiency leading to improved growth (Kromdijk *et al.*, 2016) or seed production (De Souza *et al.*, 2022), although it is not always the case (Garcia-Molina and Leister, 2020; Lehretz *et al.*, 2022). The reason for this is not clear, but the interplay between total

313 photoprotection, ability to use assimilate, and the rates of activation and relaxation are likely to
314 be important. Wang et al. (2020) previously used a ray tracing algorithm and canopy model to
315 estimate the predicted benefit of manipulating NPQ or photosynthetic induction rates in soybean
316 given available natural variation. The data used was based on preliminary measurements made
317 on the same SoyNAM panel as in this publication (Song *et al.*, 2017; Diers *et al.*, 2018).
318 However, predictions of the impact on altering NPQ relaxation were based on light-to-dark
319 measurements, which are shown to be unlikely to be realistic for a field environment (Fig. 1B)
320 and did not focus on identifying which soybean genotypes could be beneficial for genomic
321 selection from the perspective of NPQ relaxation. Here, the differences in NPQ parameters
322 between lines was smaller, ~28% difference in τ_{qE} between fastest and slowest relaxing lines as
323 compared to 40% (Wang *et al.*, 2020), which equates to 1.6% daily assimilation, likely due to
324 the much deeper sampling and measurement conditions. Analysis of the response of soybean
325 to artificial increase of photosynthesis in the field by elevation of [CO_2], show that while older
326 cultivars appear sink limited, modern cultivars appear to be source limited and can fully use any
327 increase in photosynthesis (Ainsworth and Long, 2021). Given the limited diversity of NPQ
328 relaxation rates in soybean germplasm, achieving increases in photosynthetic efficiency through
329 manipulating NPQ is likely to be best achieved through transgenic approaches.
330

Experimental procedures

Plants and growth conditions

The 41 parents of the Soybean Nested Association Mapping (NAM) population (Song et al., 2017, Diers et al., 2018) were grown in the field at the Crop Sciences Research and Education Center at the University of Illinois at Urbana-Champaign in 2021 (latitude 40.084604, longitude -88.227952) and 2022 (latitude 40.064866, longitude -88.193084). Seeds were planted in 1.2 m single-row plots with a 0.75 m row spacing, with 40 seed m^{-1} in a North-South orientation on 5 June 2021 and 13 June 2022 (Table S4). The experiment was arranged in a randomized complete block design, with five replicate plots per genotype. Standard agronomic practices were employed.

For greenhouse experiments, seeds of the NAM Recurrent Parent IA3023 were planted 2 mm deep in a Soil: Perlite:Torpedo Sand mixture (1:1:1), in classic 600 2-gallon pots on May 5th, 2021. Plants were watered and fertilized as needed, and grown under 1500 µmol m^{-2} s^{-1} light, 14 h daylength, with temperatures set a 27-30^{o}C during the day, 23-26^{o}C at night.

Meteorological data collection

Meteorological variables were measured every 30 min by a weather station at the University of Illinois Energy Farm, approximately 1 km from the Crop Sciences Research and Education Center (latitude 40.062832, longitude -88.198417). Air temperature (T_a, °C) and relative humidity (RH, %) were recorded by a HMP45C probe (Campbell Scientific, Logan, UT, USA), and incoming shortwave radiation (Fsd, W m^{-2}) was from a CNR1 radiometer (Kipp & Zonen, The Netherlands), both instruments were installed 4 m above the ground. T_a and RH were used to calculate saturation vapor pressure (e_s) and actual vapor pressure (e_a) for each 30 min period, which were then used to calculate vapor pressure deficit (VPD, kPa) as per Equations 1-3:

$$e_s = 0.6106 * exp^{(\frac{(17.27*Ta)}{(237.3+Ta)})} \quad Equation\ 1$$

$$e_a = \frac{RH * e_s}{100} \quad Equation\ 2$$

$$VPD = e_s - e_a \quad Equation\ 3$$

Occasional gaps in meteorological data are inevitable when measuring at these time scales, so data gaps were filled where needed, whereby an artificial neural network was used to generate a complete time-series with external data sourced from the University of Illinois Willard Airport

weather station (station ID: 725315-94870) and ERA-interim data from the European Centre for Medium Range Forecasts. In total, less than 5 % of data required gap filling. Daily summary values were then calculated for each variable, with T_a and VPD presented as daily mean, Fsd as daytime-only (i.e. 06:00-18:00) mean, and rainfall as a daily sum. The variables T_a_7day, VPD_7day, and Fsd_7day represent the average for the past 7 days for these values. The variable Precip_7day represent the sum in precipitation for the past 7 days. The cumulated net radiation (cumFn) was calculated as the sum of net radiation between 6:00 and 12:00

Chlorophyll fluorescence analysis

For field experiments, plants were sampled between 8:00-10:00 at seven time points across development in 2021 and six time points in 2022 (Table S5) according to (Gotarkar *et al.*, 2022). Briefly, five 4.8 mm leaf disks were collected per plot, sampling from the upper-most mature leaf using a cork borer (H9663; Humboldt Mfg. Co.). Leaf disks were then transferred face down into wells of a flat-bottomed 96 well plate (FB012929; Fisher Scientific), humidity was maintained by placing a half-wet nasal aspirator filter into each well (iHank-Nose B07P6XCTGV; Amazon), and plates were sealed and wrapped in aluminum foil followed by overnight dark adaptation. Measurements were taken with modulated chlorophyll fluorescence imaging system (CF imager; Technologica, UK). To induce low-high-low light fluctuations, samples were illuminated for 10 min at 50 µmol m^{-2} s^{-1}, followed by 15 min at 2000 µmol m^{-2} s^{-1} and 50 min of 50 µmol m^{-2} s^{-1}. $F_{m'}$, was determined by applying saturating pulses (4000 µmol m^{-2} s^{-1}) at 2.5, 5, 7.5, 10 min after the actinic light was turned on (50 µmol m^{-2} s^{-1}), 2.5, 5, 7.5, 10, 12.5 and 15 min after high light exposure (2000 µmol m^{-2} s^{-1}), and 2.5, 5, 10, 15, 20, 25, 30, 35, 40, 45 and 50 min following return to low light (50 µmol m^{-2} s^{-1}). The background was excluded manually and NPQ values at each pulse were calculated.

NPQ values were calculated for each time point using custom MatLab scripts according to (Gotarkar *et al.*, 2022). NPQ relaxation parameters A_{qE}, A_{qM}, A_{qI}, τ_{qE} and τ_{qM} were then calculated by fitting the sum of a double exponential function to measured NPQ values following shut off of the actinic light, according to Equation 4 (Dall'Osto *et al.*, 2014):

$$NPQ = A\mathrm{qI} + AqE^{\left(-\frac{t}{\tau qE}\right)} + AqM^{\left(-\frac{t}{\tau qM}\right)} \qquad Equation\ 4$$

using the fit function in MatLab R0218b, where t is the measured fluorescence at a given time point. Maximum NPQ values are defined as the maximum value reached during the 15 min illumination at high light.

Measurement of light intensity at layers in the soybean canopy

Light intensity was measured simultaneously within and above a soybean canopy using quantum sensors (LI-190R, LICOR, Lincoln, NE, USA) mounted on an aluminum frame reading at 8 different levels (9, 24, 44, 64, 84, 104, 124, and 144 cm height). Measurements were manually logged on a datalogger (CR100x; Campbell Scientific, Logan, UT, USA) after carefully placing the frame within the canopy with the sensors close to the stems and waiting for stable readings. Those measurements were taken on six different cultivars from a germplasm collection at (or close to) the reproductive stage R5. Measurements were conducted on August 17th, 2022 between 12:00 and 12:15.

3D soybean model and light distribution

The dynamics of lighting within a soybean canopy were predicted with a 3D architectural representation, using our previously presented soybean canopy model (Song et al.,2019; Wang et al., 2020). The model was parameterized on the measured architecture of soybean hub parent

IA3023 (RC) at the University of Illinois Energy Farms in August 2022 (measured canopy parameters are listed in Tables S6-8). Leaf area was measured when the soybean plants on 18th August 2021. The youngest mature leaf (~3rd trifoliate from the top) was selected for analysis, the area of all three leaves in the trifoliate from three plots was measured with a leaf area meter (LI3100C; LI-COR Environmental, Lincoln, NE, USA) (Table S6). Detailed parameters were measured for 5 genotypes on August 19th 2021 and 8 genotypes on August 30th 2022. Plant height was measured from the base to tip after the plants were cut from the base and stretched. Leaf width was measured at the widest point from each leaflet in a trifoliate and averaged. Leaf length was measured from base to tip for each trifoliate and averaged. Internode length was measured for the 6th internode from the top, with one value recorded per plant, and branch angle was measured for the 6th branch from the top using a digital protractor, one measurement per plant. The total number of trifoliate, number of primary and secondary branches and number of pods per plant were counted manually for one plant per plot (Table S7). Leaf Area Index (LAI) was measured using the SunScan canopy analysis system (SS1; Delta-T Devices Ltd, UK) with a 1 m probe according to the manufacturer's instructions.

LAI was measured at R5 developmental stage between 11:56 and 13:50 on 20th August 2021 on both sides of each plot and averaged, with the probe positioned parallel to the rows (Table S8). To calculate the actual light environment of the soybean canopy, measured PAR data on DOY 226 and 227 of 2021 in Bondville, IL. (Earth System Research Laboratory, Global Monitoring Division https://www.esrl.noaa.gov/gmd/grad/surfrad/dataplot.html) was incorporated (Table S9). A forward ray-tracing algorithm (FastTracer; Song et al. 2013) was used to predict the light absorption of each leaf pixel (ca. 5 mm^2) every 1min from 05:00 – 19:00 in Champaign IL, US (40.11N, 88.21 W).

Simulation of dynamic photosynthesis

Dynamic photosynthetic rates were calculated for every 10 s (Δt) of the day using the absorbed light for each leaf pixel, considering rates of Rubisco activation and NPQ relaxation (Wang et al., 2020). Then the canopy net CO_2 uptake (A_c) was calculated as:

$$A_c(t) = \frac{\sum (A_i(t) \cdot S_i)}{S_{ground}} \quad 440$$

Where $A_i(t)$ is the CO_2 uptake rate of a leaf pixel; S_i is the surface area of each pixel, S_{ground} represents the occupied ground area of the simulated canopy. All simulations were conducted in MATLAB 2021a (The Mathworks, Inc®).

Time constants of NPQ relaxation and Rubisco activation across the NAM population were measured and used as input of the dynamic photosynthetic model (model inputs were listed in Table S10). The time constant of Rubisco de-activation was assumed to be double the time required for activation for each genotype (Taylor & Long, 2017).

Statistical Analysis

Technical replicates from the chlorophyll fluorescence analysis were averaged prior to statistical analyses. The impact of genotypes, the environment, and their interaction on NPQ relaxation was assessed by fitting an ANOVA model in R v4.1.2 (R Core Team, 2016) and RStudio v2024.04.0 (RStudio Team, 2015) using the stats R package v4.1.2. The ANOVA model was written as NPQ parameter ~ genotype (G) + day (or the environment, E) + genotype * day with G and E set as fixed factors. The impact of the environment was assessed for each NPQ relaxation parameter by using a stepwise regression model to determine which environmental variables had the strongest impact on the parameters. The initial linear model included all the

environmental variables. A both-direction stepwise algorithm then tested the model by removing and re-including environmental variables one by one. The Akaike's information criterion (AIC) was used to select the best minimum adequate model (lowest AIC) using the stats R package v4.1.2. This test was performed with data collected in 2021, 2022, and for the two years together. Centered and scaled environmental variables were used as input in the model. The relationships between genotypes, the environment, and NPQ relaxation were explored using canonical correlation analysis (CCA). This multivariate statistical approach identifies linear combinations of variables for the two datasets (here, NPQ and environmental data) to construct a pair of canonical variates that are maximally correlated with each other on the first canonical axis (CC1). Then, a second pair of canonical variates is made with a maximized correlation on the second canonical axis (CC2) but uncorrelated with the CC1. The process is repeated for each canonical variates' pairs. A significant correlation between pairs enables associations among the different variables. The CCA analysis was performed in R using the CCA R package v1.2.1 (González and Déjean, 2021). The statistical significance of canonical correlation coefficients was carried out by using Wilks' Lambda with the CCP R package v1.2 (Menzel, 2022). All NPQ relaxation parameters were used as input for the first dataset. Environmental variables were used as input for the second dataset with the exception of VPD_7day, Precip_7day, Fsd_7day, and cumulated precipitation based on the stepwise regression model to reduce co-linearity.

For chlorophyll fluorescence analysis, leaf disks with F_v/F_m value <0.75 were excluded to ensure measured values were from healthy disks representative of whole plant kinetics. Additional outliers were defined and removed if calculated parameter values were <0. The effect of genotypic differences from the RC for each NPQ relaxation parameter were estimated using linear mixed-effects models (Bates *et al.*, 2015). Linear fixed effects included days, air temperature (Ta), vapor pressure deficit (VPD), precipitation (Precip), incoming shortwave radiation (Fsd), a 7-day rolling mean air temperature (Ta 7day), and a 7-day rolling mean vapor pressure deficit (VPD 7day), with random effects for plot and leaf disks (Data S1). Akaike's Information Criterion (AIC) was used to compare linear mixed-effects models (Akaike, 1974; Faraway, 2016). Briefly, nested model comparisons via AIC determined which genotypes exhibit different measures from the baseline genotype RC, following a procedure to fit a smaller model with one genotype removed. This smaller model assumes that there is no difference between that genotype and the RC baseline. The computed AIC value for this smaller model was compared with the AIC value of the full model with all genotypes considered. If the smaller

model has a lower AIC value, then the removed genotype does not exhibit an effect on NPQ relaxation parameters that is different from the RC baseline. This procedure was repeated for all genotypes and all linear mixed-effects models involving NPQ relaxation parameters as a response. In addition to this approach, a principal component analysis (PCA) was performed for each days separately to identify any patterns among NAM groups (i,e, diverse, elite, PI, and RC) and/or notable genotypes. The analysis was performed using the ade4 (v1.7-22) R package (Dray and Dufour, 2007). Centered and scaled NPQ parameters were used as input variables. Differences between NAM groups in their principal component coordinates were assessed by using a one-way ANOVA with groups as a fixed factor with the R stats package (v4.1.2).

Data Statement and Accession Numbers

All raw NPQ data values prior to filtering and processing are provided in csv format in Table S1. All raw chlorophyll fluorescence imager files and custom scripts can be accessed via FigShare 10.6084/m9.figshare.21574509 and 10.6084/m9.figshare.25939504.

Acknowledgements

We thank Troy Cary for setting up the soybean NAM population plots; Wanne Kromdijk for help setting up scripts for analysis of NPQ relaxation parameters; Caitlin Moore for assistance with data from 2018 and 2019 used in previous versions of this manuscript; Meghan Burns, Meghan Blaszynski, Jacob Milo, and Abigail Hinkle for their assistance collecting samples and Stephen P. Long for commenting and feedback on the manuscript. This work was supported by the project Realizing Increased Photosynthetic Efficiency (RIPE), funded from 2017-2023 by the Bill and Melinda Gates Foundation (BMGF), Foundation for Food and Agriculture Research (FFAR) and the UK Department for International Development (UKAid) under grant number OPP117215. SJB was supported by Carl R. Woese Institute for Genomic Biology Fellowship.

Short legends for Supporting Information

Table S1: Raw NPQ timeseries values for all technical replicates prior to filtering and processing.

Table S2. Calculated NPQ relaxation parameters for all plots and genotypes.

Table S3. Genotype means for calculated NPQ relaxation parameters combining all data from 2021 and 2022.

Table S4: Field design with plot numbers and orientation in 2021 and 2022.

Table S5. Sampling time points in 2021 and 2022 including days after sowing and development stage.

Table S6. Leaf area measurements for 41 SoyNAM founders recorded in 2022, data is provided for three biological replicates.

Table S7. Canopy measurements for seven SoyNAM founders and reference genotype RC recorded on August 30th 2022.

Table S8. Leaf area index measurements for 41 SoyNAM founders recorded in 2022, data is provided for two technical and 5 biological replicates.

Table S9. Measured PAR values on day of the year (DOY) 226 and 227 of 2021 in Bondville, IL. Earth System Research Laboratory, Global Monitoring Division.

Table S10. Input values for 3D canopy model.

Data S1. Description of statistical analysis comparing NPQ relaxation kinetics between genotypes.

Conflict of Interest

The authors report no conflicts of interest.

References

Ainsworth, E.A. and Long, S.P. (2021) 30 years of free-air carbon dioxide enrichment (FACE): What have we learned about future crop productivity and its potential for adaptation? *Glob. Change Biol.*, **27**, 27–49. Available at: https://doi.org/10.1111/gcb.15375 [Accessed January 26, 2024].

Akaike, H. (1974) A new look at the statistical model identification. *IEEE Trans. Autom. Control*, **19**, 716–723.

Bates, D., Mächler, M., Bolker, B. and Walker, S. (2015) Fitting Linear Mixed-Effects Models Using lme4. *J. Stat. Softw.*, **67**, 1–48. Available at: https://www.jstatsoft.org/index.php/jss/article/view/v067i01 [Accessed March 8, 2024].

Bethmann, S., Melzer, M., Schwarz, N. and Jahns, P. (2019) The zeaxanthin epoxidase is degraded along with the D1 protein during photoinhibition of photosystem II. *Plant Direct*, **3**, e00185. Available at: https://doi.org/10.1002/pld3.185 [Accessed May 30, 2024].

Burgess, A.J., Gibbs, J.A. and Murchie, E.H. (2019) A canopy conundrum: can wind-induced movement help to increase crop productivity by relieving photosynthetic limitations? *J. Exp. Bot.*, **70**, 2371–2380. Available at: https://doi.org/10.1093/jxb/ery424 [Accessed February 16, 2023].

Cowling, S.B., Treeintong, P., Ferguson, J., Soltani, H., Swarup, R., Mayes, S. and Murchie, E.H. (2022) Out of Africa: characterizing the natural variation in dynamic photosynthetic traits in a diverse population of African rice (Oryza glaberrima). *J. Exp. Bot.*, **73**, 3283–3298. Available at: https://doi.org/10.1093/jxb/erab459 [Accessed October 27, 2023].

Dall'Osto, L., Cazzaniga, S., Wada, M. and Bassi, R. (2014) On the origin of a slowly reversible fluorescence decay component in the Arabidopsis npq4 mutant. *Philos. Trans. R. Soc. B Biol. Sci.*, **369**, 20130221. Available at: https://doi.org/10.1098/rstb.2013.0221 [Accessed March 17, 2023].

Davison, P.A., Hunter, C.N. and Horton, P. (2002) Overexpression of β-carotene hydroxylase enhances stress tolerance in Arabidopsis. *Nature*, **418**, 203–206. Available at: https://doi.org/10.1038/nature00861.

De Souza, A.P., Burgess, S.J., Doran, L., et al. (2022) Soybean photosynthesis and crop yield are improved by accelerating recovery from photoprotection. *Science*, **377**, 851–854. Available at: https://doi.org/10.1126/science.adc9831 [Accessed December 20, 2022].

Demmig-Adams, B. (1998) Survey of Thermal Energy Dissipation and Pigment Composition in Sun and Shade Leaves. *Plant Cell Physiol.*, **39**, 474–482. Available at: https://doi.org/10.1093/oxfordjournals.pcp.a029394 [Accessed March 6, 2024].

Demmig-Adams, B. and Adams III, W.W. (2006) Photoprotection in an ecological context: the remarkable complexity of thermal energy dissipation. *New Phytol.*, **172**, 11–21. Available at: https://doi.org/10.1111/j.1469-8137.2006.01835.x [Accessed May 29, 2024].

583 **Demmig-Adams, B., Cohu, C.M., Muller, O. and Adams, W.W.** (2012) Modulation of
584 photosynthetic energy conversion efficiency in nature: from seconds to seasons.
585 *Photosynth. Res.*, **113**, 75–88. Available at: https://doi.org/10.1007/s11120-012-9761-6.

586 **Demmig-Adams, B., Polutchko, S.K., Stewart, J.J. and Adams, W.W.** (2022) History of
587 excess-light exposure modulates extent and kinetics of fast-acting non-photochemical
588 energy dissipation. *Plant Physiol. Rep.*, **27**, 560–572. Available at:
589 https://doi.org/10.1007/s40502-022-00689-2.

590 **Diers, B.W., Specht, J., Rainey, K.M., et al.** (2018) Genetic Architecture of Soybean Yield and
591 Agronomic Traits. *G3 GenesGenomesGenetics*, **8**, 3367.

592 **Dray, S. and Dufour, A.-B.** (2007) The ade4 Package: Implementing the Duality Diagram for
593 Ecologists. *J. Stat. Softw.*, **22**, 1–20. Available at:
594 https://www.jstatsoft.org/index.php/jss/article/view/v022i04 [Accessed May 29, 2024].

595 **Faraway, J.J.** (2016) *Extending the Linear Model with R: Generalized Linear, Mixed Effects and*
596 *Nonparametric Regression Models* Second Edition., New York, NY: Chapman and
597 Hall/CRC. Available at: https://doi.org/10.1201/9781315382722.

598 **Garcia-Molina, A. and Leister, D.** (2020) Accelerated relaxation of photoprotection impairs
599 biomass accumulation in Arabidopsis. *Nat. Plants*, **6**, 9–12. Available at:
600 https://doi.org/10.1038/s41477-019-0572-z.

601 **Gizlice, Z., Carter Jr., T.E. and Burton, J.W.** (1994) Genetic Base for North American Public
602 Soybean Cultivars Released between 1947 and 1988. *Crop Sci.*, **34**,
603 cropsci1994.0011183X003400050001x. Available at:
604 https://doi.org/10.2135/cropsci1994.0011183X003400050001x [Accessed March 27,
605 2024].

606 **González, I. and Déjean, S.** (2021) CCA: Canonical Correlation Analysis. Available at:
607 https://CRAN.R-project.org/package=CCA.

608 **Gotarkar, D., Doran, L., Burns, M., Hinkle, A., Kromdijk, J. and Burgess, S.J.** (2022) High-
609 Throughput Analysis of Non-Photochemical Quenching in Crops Using Pulse Amplitude
610 Modulated Chlorophyll Fluorometry. *J. Vis. Exp. JoVE*. Available at:
611 http://europepmc.org/abstract/MED/35876527.

612 **Grieco, M., Roustan, V., Dermendjiev, G., et al.** (2020) Adjustment of photosynthetic activity
613 to drought and fluctuating light in wheat. *Plant Cell Environ.*, **43**, 1484–1500. Available
614 at: https://doi.org/10.1111/pce.13756 [Accessed May 29, 2024].

615 **Herritt, M., Dhanapal, A.P. and Fritschi, F.B.** (2016) Identification of Genomic Loci Associated
616 with the Photochemical Reflectance Index by Genome-Wide Association Study in
617 Soybean. *Plant Genome*, **9**. Available at:
618 http://dx.doi.org/10.3835/plantgenome2015.08.0072.

619 **Herritt, M., Dhanapal, A.P., Purcell, L.C. and Fritschi, F.B.** (2018) Identification of genomic
620 loci associated with 21chlorophyll fluorescence phenotypes by genome-wide association
621 analysis in soybean. *BMC Plant Biol.*, **18**, 312.

Hubbart, S., Smillie, I.R.A., Heatley, M., Swarup, R., Foo, C.C., Zhao, L. and Murchie, E.H. (2018) Enhanced thylakoid photoprotection can increase yield and canopy radiation use efficiency in rice. *Commun. Biol.*, **1**, 22. Available at: https://doi.org/10.1038/s42003-018-0026-6.

Hyten, D.L., Song, Q., Zhu, Y., Choi, I.-Y., Nelson, R.L., Costa, J.M., Specht, J.E., Shoemaker, R.C. and Cregan, P.B. (2006) Impacts of genetic bottlenecks on soybean genome diversity. *Proc. Natl. Acad. Sci.*, **103**, 16666–16671. Available at: https://doi.org/10.1073/pnas.0604379103 [Accessed March 10, 2024].

Jahns, P. and Holzwarth, A.R. (2012) The role of the xanthophyll cycle and of lutein in photoprotection of photosystem II. *Photosyst. II*, **1817**, 182–193. Available at: https://www.sciencedirect.com/science/article/pii/S0005272811000971.

Jung, H.-S. and Niyogi, K.K. (2009) Quantitative Genetic Analysis of Thermal Dissipation in Arabidopsis. *Plant Physiol.*, **150**, 977.

Kaiser, E., Correa Galvis, V. and Armbruster, U. (2019) Efficient photosynthesis in dynamic light environments: a chloroplast's perspective. *Biochem. J.*, **476**, 2725–2741. Available at: https://doi.org/10.1042/BCJ20190134 [Accessed October 27, 2023].

Kaiser, E., Morales, A. and Harbinson, J. (2018) Fluctuating Light Takes Crop Photosynthesis on a Rollercoaster Ride. *Plant Physiol.*, **176**, 977–989. Available at: https://doi.org/10.1104/pp.17.01250 [Accessed October 28, 2023].

Kasajima, I., Ebana, K., Yamamoto, T., Takahara, K., Yano, M., Kawai-Yamada, M. and Uchimiya, H. (2011) Molecular distinction in genetic regulation of nonphotochemical quenching in rice. *Proc. Natl. Acad. Sci.*, **108**, 13835.

Kiss, A.Z., Ruban, A.V. and Horton, P. (2008) The PsbS Protein Controls the Organization of the Photosystem II Antenna in Higher Plant Thylakoid Membranes*. *J. Biol. Chem.*, **283**, 3972–3978. Available at: https://www.sciencedirect.com/science/article/pii/S002192582069706X.

Kofsky, J., Zhang, H. and Song, B.-H. (2018) The Untapped Genetic Reservoir: The Past, Current, and Future Applications of the Wild Soybean (Glycine soja). *Front. Plant Sci.*, **9**. Available at: https://www.frontiersin.org/journals/plant-science/articles/10.3389/fpls.2018.00949.

Kramer, D.M. and Evans, J.R. (2011) The Importance of Energy Balance in Improving Photosynthetic Productivity. *Plant Physiol.*, **155**, 70–78. Available at: https://doi.org/10.1104/pp.110.166652 [Accessed October 28, 2023].

Krause, G.H., Vernotte, C. and Briantais, J.-M. (1982) Photoinduced quenching of chlorophyll fluorescence in intact chloroplasts and algae. Resolution into two components. *Biochim. Biophys. Acta BBA - Bioenerg.*, **679**, 116–124. Available at: https://www.sciencedirect.com/science/article/pii/0005272882902626.

Kress, E. and Jahns, P. (2017) The Dynamics of Energy Dissipation and Xanthophyll Conversion in Arabidopsis Indicate an Indirect Photoprotective Role of Zeaxanthin in Slowly Inducible and Relaxing Components of Non-photochemical Quenching of

662 Excitation Energy. *Front. Plant Sci.*, **8**. Available at:
663 https://www.frontiersin.org/journals/plant-science/articles/10.3389/fpls.2017.02094.

664 **Kromdijk, J., Głowacka, K., Leonelli, L., Gabilly, S.T., Iwai, M., Niyogi, K.K. and Long, S.P.**
665 (2016) Improving photosynthesis and crop productivity by accelerating recovery from
666 photoprotection. *Science*, **354**, 857–861. Available at:
667 https://doi.org/10.1126/science.aai8878 [Accessed December 20, 2022].

668 **Lehretz, G.G., Schneider, A., Leister, D. and Sonnewald, U.** (2022) High non-photochemical
669 quenching of VPZ transgenic potato plants limits CO2 assimilation under high light
670 conditions and reduces tuber yield under fluctuating light. *J. Integr. Plant Biol.*, **64**, 1821–
671 1832. Available at: https://doi.org/10.1111/jipb.13320 [Accessed November 8, 2023].

672 **Leister, D.** (2023) Enhancing the light reactions of photosynthesis: Strategies, controversies,
673 and perspectives. *"Celebrating 15 Years Publ. Spec. Issue*, **16**, 4–22. Available at:
674 https://www.sciencedirect.com/science/article/pii/S1674205222002684.

675 **Lopez, M.A., Xavier, A. and Rainey, K.M.** (2019) Phenotypic Variation and Genetic
676 Architecture for Photosynthesis and Water Use Efficiency in Soybean (Glycine max L.
677 Merr). *Front. Plant Sci.*, **10**. Available at: https://www.frontiersin.org/journals/plant-
678 science/articles/10.3389/fpls.2019.00680.

679 **Menzel, U.** (2022) CCP: Significance Tests for Canonical Correlation Analysis (CCA). Available
680 at: https://cran.r-project.org/web/packages/CCP/index.html.

681 **Montes, C.M., Fox, C., Sanz-Sáez, Á., et al.** (2022) High-throughput characterization,
682 correlation, and mapping of leaf photosynthetic and functional traits in the soybean
683 (Glycine max) nested association mapping population. *Genetics*, **221**, iyac065. Available
684 at: https://doi.org/10.1093/genetics/iyac065 [Accessed March 4, 2024].

685 **Nilkens, M., Kress, E., Lambrev, P., Miloslavina, Y., Müller, M., Holzwarth, A.R. and Jahns,**
686 **P.** (2010) Identification of a slowly inducible zeaxanthin-dependent component of non-
687 photochemical quenching of chlorophyll fluorescence generated under steady-state
688 conditions in Arabidopsis. *Biochim. Biophys. Acta BBA - Bioenerg.*, **1797**, 466–475.
689 Available at: https://www.sciencedirect.com/science/article/pii/S0005272810000022.

690 **Niyogi, K.K., Grossman, A.R. and Björkman, O.** (1998) Arabidopsis Mutants Define a Central
691 Role for the Xanthophyll Cycle in the Regulation of Photosynthetic Energy Conversion.
692 *Plant Cell*, **10**, 1121–1134. Available at: https://doi.org/10.1105/tpc.10.7.1121 [Accessed
693 April 16, 2024].

694 **Pashayeva, A., Wu, G., Huseynova, I., Lee, C.-H. and Zulfugarov, I.S.** (2021) Role of
695 Thylakoid Protein Phosphorylation in Energy-Dependent Quenching of Chlorophyll
696 Fluorescence in Rice Plants. *Int. J. Mol. Sci.*, **22**.

697 **Patricia Müller, Li, X.-P. and Niyogi, K.K.** (2001) Non-Photochemical Quenching. A Response
698 to Excess Light Energy. *Plant Physiol.*, **125**, 1558–1566. Available at:
699 http://www.jstor.org/stable/4279788 [Accessed November 8, 2023].

Pinnola, A. and Bassi, R. (2018) Molecular mechanisms involved in plant photoprotection. *Biochem. Soc. Trans.*, **46**, 467–482. Available at: https://doi.org/10.1042/BST20170307 [Accessed October 28, 2023].

Pollastri, S., Jorba, I., Hawkins, T.J., et al. (2019) Leaves of isoprene-emitting tobacco plants maintain PSII stability at high temperatures. *New Phytol.*, **223**, 1307–1318. Available at: https://doi.org/10.1111/nph.15847 [Accessed May 29, 2024].

Porcar-Castell, A. (2011) A high-resolution portrait of the annual dynamics of photochemical and non-photochemical quenching in needles of Pinus sylvestris. *Physiol. Plant.*, **143**, 139–153. Available at: https://doi.org/10.1111/j.1399-3054.2011.01488.x [Accessed March 18, 2024].

R Core Team (2016) R: A language and environment for statistical computing. Available at: https://www.R-project.org/.

Robakowski, P. and Wyka, T. (2009) Winter photoinhibition in needles of Taxus baccata seedlings acclimated to different light levels. *Photosynthetica*, **47**, 527–535. Available at: https://ps.ueb.cas.cz/artkey/phs-200904-0006.php.

RStudio Team (2015) RStudio: Integrated development for R. Available at: RStudio Team.

Ruban, A.V., Johnson, M.P. and Duffy, C.D.P. (2012) The photoprotective molecular switch in the photosystem II antenna. *Photosyst. II*, **1817**, 167–181. Available at: https://www.sciencedirect.com/science/article/pii/S0005272811000910.

Ruban, A.V. and Wilson, S. (2021) The Mechanism of Non-Photochemical Quenching in Plants: Localization and Driving Forces. *Plant Cell Physiol.*, **62**, 1063–1072. Available at: https://doi.org/10.1093/pcp/pcaa155 [Accessed November 8, 2023].

Rungrat, T., Almonte, A.A., Cheng, R., Gollan, P.J., Stuart, T., Aro, E.-M., Borevitz, J.O., Pogson, B. and Wilson, P.B. (2019) A Genome-Wide Association Study of Non-Photochemical Quenching in response to local seasonal climates in Arabidopsis thaliana. *Plant Direct*, **3**, e00138–e00138.

Sacharz, J., Giovagnetti, V., Ungerer, P., Mastroianni, G. and Ruban, A.V. (2017) The xanthophyll cycle affects reversible interactions between PsbS and light-harvesting complex II to control non-photochemical quenching. *Nat. Plants*, **3**, 16225. Available at: https://doi.org/10.1038/nplants.2016.225.

Sahay, S., Grzybowski, M., Schnable, J.C. and Głowacka, K. (2023) Genetic control of photoprotection and photosystem II operating efficiency in plants. *New Phytol.*, **239**, 1068–1082. Available at: https://doi.org/10.1111/nph.18980 [Accessed October 27, 2023].

Sakoda, K., Adachi, S., Yamori, W. and Tanaka, Y. (2022) Towards improved dynamic photosynthesis in C3 crops by utilizing natural genetic variation. *J. Exp. Bot.*, **73**, 3109–3121. Available at: https://doi.org/10.1093/jxb/erac100 [Accessed October 27, 2023].

Schaller, S., Latowski, D., Jemioła-Rzemińska, M., Wilhelm, C., Strzałka, K. and Goss, R. (2010) The main thylakoid membrane lipid monogalactosyldiacylglycerol (MGDG)

promotes the de-epoxidation of violaxanthin associated with the light-harvesting complex of photosystem II (LHCII). *Biochim. Biophys. Acta BBA - Bioenerg.*, **1797**, 414–424. Available at: https://www.sciencedirect.com/science/article/pii/S0005272809003065.

Schwarz, N., Armbruster, U., Iven, T., Brückle, L., Melzer, M., Feussner, I. and Jahns, P. (2015) Tissue-Specific Accumulation and Regulation of Zeaxanthin Epoxidase in Arabidopsis Reflect the Multiple Functions of the Enzyme in Plastids. *Plant Cell Physiol.*, **56**, 346–357. Available at: https://doi.org/10.1093/pcp/pcu167 [Accessed April 17, 2024].

Soleh, M.A., Tanaka, Y., Kim, S.Y., Huber, S.C., Sakoda, K. and Shiraiwa, T. (2017) Identification of large variation in the photosynthetic induction response among 37 soybean [Glycine max (L.) Merr.] genotypes that is not correlated with steady-state photosynthetic capacity. *Photosynth. Res.*, **131**, 305–315. Available at: https://doi.org/10.1007/s11120-016-0323-1.

Song, Q., Yan, L., Quigley, C., et al. (2017) Genetic Characterization of the Soybean Nested Association Mapping Population. *Plant Genome*, **10**. Available at: http://dx.doi.org/10.3835/plantgenome2016.10.0109.

Sun, Z., Shen, Y. and Niinemets, Ü. (2020) Responses of isoprene emission and photochemical efficiency to severe drought combined with prolonged hot weather in hybrid Populus. *J. Exp. Bot.*, **71**, 7364–7381. Available at: https://doi.org/10.1093/jxb/eraa415 [Accessed March 18, 2024].

Wang, Q., Zhao, H., Jiang, J., Xu, J., Xie, W., Fu, X., Liu, C., He, Y. and Wang, G. (2017) Genetic Architecture of Natural Variation in Rice Nonphotochemical Quenching Capacity Revealed by Genome-Wide Association Study. *Front. Plant Sci.*, **8**. Available at: https://www.ncbi.nlm.nih.gov/pmc/articles/PMC5645755/ [Accessed April 23, 2018].

Wang, Y., Burgess, S.J., Becker, E.M. de and Long, S.P. (2020) Photosynthesis in the fleeting shadows: an overlooked opportunity for increasing crop productivity? *Plant J.*, **101**, 874–884. Available at: https://doi.org/10.1111/tpj.14663 [Accessed November 8, 2023].

Watanabe, S., Xia, Z., Hideshima, R., et al. (2011) A Map-Based Cloning Strategy Employing a Residual Heterozygous Line Reveals that the GIGANTEA Gene Is Involved in Soybean Maturity and Flowering. *Genetics*, **188**, 395–407. Available at: https://doi.org/10.1534/genetics.110.125062 [Accessed April 5, 2024].

Xavier, A., Hall, B., Hearst, A.A., Cherkauer, K.A. and Rainey, K.M. (2017) Genetic Architecture of Phenomic-Enabled Canopy Coverage in Glycine max. *Genetics*, **206**, 1081–1089. Available at: https://doi.org/10.1534/genetics.116.198713 [Accessed April 5, 2024].

Zhu, J.-J., Zhang, J.-L., Liu, H.-C. and Cao, K.-F. (2009) Photosynthesis, non-photochemical pathways and activities of antioxidant enzymes in a resilient evergreen oak under different climatic conditions from a valley-savanna in Southwest China. *Physiol. Plant.*, **135**, 62–72. Available at: https://doi.org/10.1111/j.1399-3054.2008.01171.x [Accessed March 18, 2024].

779 **Zhu, X.-G., Ort, D.R., Whitmarsh, J. and Long, S.P.** (2004) The slow reversibility of
780 photosystem II thermal energy dissipation on transfer from high to low light may cause
781 large losses in carbon gain by crop canopies: a theoretical analysis. *J. Exp. Bot.*, **55**,
782 1167–1175. Available at: http://www.jstor.org/stable/24030500 [Accessed October 27,
783 2023].

784

Tables

Table 1. *List of Abbreviations*

Symbol	Description
F_v/F_m	Maximum potential quantum efficiency of Photosystem II
qE	Fast phase of NPQ relaxation, energy-dependent quenching (< 2 min)
qM	Intermediate phase of NPQ relaxation (2-30 min)
qI	Slow phase of NPQ relaxation (> 30 min)
A_{qE}	Amplitude of qE
A_{qM}	Amplitude of qM
A_{qI}	Amplitude of qI
τ_{qE}	Time constant of qE relaxation
τ_{qM}	Time constant of qM relaxation
Max. NPQ	Maximum recorded value of NPQ during experiment
F_{sd}	Incoming shortwave radiation
T_a	Air temperature
VPD	Vapor pressure deficit
AIC	Akaike's Information Criterion

788 Table 2. Table of F-test P-values obtained by fitting an ANOVA model for each NPQ relaxation
789 parameters with the genotypes (G) and days (or environment, E) set as fixed factors (i.e.,
790 variable ~ Day + Genotype + Day * Genotype).

Variable	**G**	**E**	**GxE**
A_{qI}	<0.001	<0.001	0.8325
A_{qE}	<0.001	<0.001	0.9754
τ_{qE}	<0.001	<0.001	0.1193
A_{qM}	<0.001	<0.001	0.9613
τ_{qM}	<0.001	<0.001	0.9463
Max. NPQ	<0.001	<0.001	0.8849

791

Table 3. Canonical correlations between pairs and associated Wilks lambda tests for the years 2021 and 2022.

	Canonical pairs for 2021			Canonical pairs for 2022		
	CC1	**CC2**	**CC3**	**CC1**	**CC2**	**CC3**
Can. Corr.	0.667	0.513	0.397	0.76	0.491	0.393
Wilks	0.331	0.597	0.81	0.258	0.61	0.804
F	44.83	28.458	17.562	44.724	21.473	14.364
df	36	25	16	36	25	16
p-value	<0.001	<0.001	<0.001	<0.001	<0.001	<0.001

796 Table 4. Table of F-test P-values obtained from a one-way ANOVA on the principal component
797 (PC) coordinates with the NAM population groups set as a fixed factor (i.e., PC ~ Groups).
798

Day	PC1	PC2	PC3
6/24/2021	0.1857	0.0378	0.8604
6/30/2021	0.577	0.9843	0.2048
7/7/2021	0.8924	0.9776	0.7902
7/13/2021	0.1689	0.3434	0.0026
7/20/2021	0.1532	0.3742	0.6809
7/28/2021	0.6763	0.1174	0.5885
8/11/2021	0.1156	0.3003	0.3555
7/6/2022	0.1556	0.2845	0.0379
7/12/2022	0.132	0.9386	0.5951
7/19/2022	0.4572	0.1662	0.5331
7/26/2022	0.4417	0.3223	0.3501
8/4/2022	0.9584	0.0289	0.5888
8/20/2022	0.049	0.7222	0.2524

799

800 Table 5. Summary of 41 NAM founder genotype NPQ relaxation parameters.

801 Data represent comparison of mean values per genotype across all samples.

Parameter	Range	Median
A_{qE}	01.83-02.09	01.96
τ_{qE}	00.93-01.29	01.05
A_{qM}	01.50-01.71	01.58
τ_{qM}	19.95-29.23	23.51
A_{qI}	00.38-00.60	00.47
Max. NPQ	03.81-04.22	04.02

802

803

804 **Figure Legends**

805 Figure 1: Comparison of NPQ relaxation kinetics and weather conditions over the course of two
806 field seasons, showing field level summaries of (a) 2021 and (b) 2022. Violin plots are combined
807 plot-level averages for all SoyNAM genotypes on a given sampling day. Sampling dates are
808 indicated by grey dotted lines. Precipitation is represented as cumulative values from the
809 beginning of the year, whereas VPD and Fsd are mean daily values.
810
811 Figure 2. Coefficients for the best minimum adequate model (lowest AIC) for each NPQ
812 relaxation parameters in 2021 and 2022. The R^2 and p-value are shown for each model.
813
814 Figure 3. Canonical correlation analysis (CCA) displaying the relationships between the NPQ
815 relaxation parameters and the environmental variables in (a-d) 2021 and (e-h) 2022. (a-b, e-f)
816 CCA showing the spatial distribution of the different observations on the canonical axis (CC).
817 The average (+-standard deviation) for the different NAM groups (with diverse, elite, PI, and RC
818 groups in grey, orange, blue and black, respectively) at different days is represented by different
819 shapes. For each group, a solid line connects those points to represent their evolution
820 throughout the season. (c-d, g-h) The correlation circle showing the relationships between
821 variables. Variables related to the NPQ relaxation parameters, and the environments are
822 represented in red and blue, respectively. The canonical correlation and associated statistics
823 are shown in table 4.
824
825 Figure 4. Comparison of NPQ relaxation kinetics in 41 founder genotypes of the SoyNAM
826 population and common parent. Boxplots of six calculated NPQ relaxation parameters (A_{qE}, A_{qM},
827 A_{ql}, τ_{qE}, τ_{qM}, maximum NPQ), plots are colored based on genotype group: Elite (yellow), Diverse
828 (grey), PI (blue). Dotted black lines represent the median, upper and lower bounds of the
829 interquartile range of reference line RC.
830
831 Figure 5. Summary representation of AIC trials for significant difference between genotypes and
832 the common parent (RC). Genotypes which showed a consistently larger (orange) or smaller
833 (blue) values in all six model comparisons are shown. Larger values for τ_{qE} and τ_{qM} represent
834 slower relaxation.
835
836 Figure 6. Canopy simulations comparing impact of SoyNAM phenotypic variability in NPQ
837 relaxation kinetics on carbon assimilation on an intermittently cloudy day and sunny day.

838 Measured light intensity on an intermittently cloudy day 266 (A) and sunny day 227 (B) in Illinois
839 in 2021. (C) Representation of canopy model. (D) Illustrated are losses in Ac resulting from the
840 measured rates of τ_{qE} and τ_{qM} comparing the slowest, fastest, mean and RC values from the
841 SoyNAM population on a cloudy (orange bars) and sunny (blue bars) day.
842
843 **Supplemental Figure Legends**
844 Figure S1. Coefficients for the best minimum adequate model (lowest AIC) for each NPQ
845 relaxation parameters in 2021 and 2022 combined. The R^2 and p-value are shown for each
846 model.
847
848 Figure S2. PCA of NPQ relaxation in the NAM population on 6/24/21. Diverse, elite, and PI lines
849 are shown in grey, orange, and blue, respectively. Coordinates for replicate measurements on
850 the same line were averaged. RC line is shown in black. Error bars represent the standard
851 deviation. Lines with a z-score>2.5 for one of their components were labeled.
852
853 Figure S3. PCA of NPQ relaxation in the NAM population on 6/30/21. Diverse, elite, and PI lines
854 are shown in grey, orange, and blue, respectively. Coordinates for replicate measurements on
855 the same line were averaged. RC line is shown in black. Error bars represent the standard
856 deviation. Lines with a z-score>2.5 for one of their components were labeled.
857
858 Figure S4. PCA of NPQ relaxation in the NAM population on 7/7/21. Diverse, elite, and PI lines
859 are shown in grey, orange, and blue, respectively. Coordinates for replicate measurements on
860 the same line were averaged. RC line is shown in black. Error bars represent the standard
861 deviation. Lines with a z-score>2.5 for one of their components were labeled.
862
863 Figure S5. PCA of NPQ relaxation in the NAM population on 7/13/21. Diverse, elite, and PI lines
864 are shown in grey, orange, and blue, respectively. Coordinates for replicate measurements on
865 the same line were averaged. RC line is shown in black. Error bars represent the standard
866 deviation. Lines with a z-score>2.5 for one of their components were labeled.
867
868 Figure S6. PCA of NPQ relaxation in the NAM population on 7/20/21. Diverse, elite, and PI lines
869 are shown in grey, orange, and blue, respectively. Coordinates for replicate measurements on
870 the same line were averaged. RC line is shown in black. Error bars represent the standard
871 deviation.

Figure S7. PCA of NPQ relaxation in the NAM population on 7/28/21. Diverse, elite, and PI lines are shown in grey, orange, and blue, respectively. Coordinates for replicate measurements on the same line were averaged. RC line is shown in black. Error bars represent the standard deviation.

Figure S8. PCA of NPQ relaxation in the NAM population on 8/11/21. Diverse, elite, and PI lines are shown in grey, orange, and blue, respectively. Coordinates for replicate measurements on the same line were averaged. RC line is shown in black. Error bars represent the standard deviation.

Figure S9. PCA of NPQ relaxation in the NAM population on 7/6/22. Diverse, elite, and PI lines are shown in grey, orange, and blue, respectively. Coordinates for replicate measurements on the same line were averaged. RC line is shown in black. Error bars represent the standard deviation.

Figure S10. PCA of NPQ relaxation in the NAM population on 7/12/22. Diverse, elite, and PI lines are shown in grey, orange, and blue, respectively. Coordinates for replicate measurements on the same line were averaged. RC line is shown in black. Error bars represent the standard deviation.

Figure S11. PCA of NPQ relaxation in the NAM population on 7/19/22. Diverse, elite, and PI lines are shown in grey, orange, and blue, respectively. Coordinates for replicate measurements on the same line were averaged. RC line is shown in black. Error bars represent the standard deviation.

Figure S12. PCA of NPQ relaxation in the NAM population on 7/26/22. Diverse, elite, and PI lines are shown in grey, orange, and blue, respectively. Coordinates for replicate measurements on the same line were averaged. RC line is shown in black. Error bars represent the standard deviation.

Figure S13. PCA of NPQ relaxation in the NAM population on 8/4/22. Diverse, elite, and PI lines are shown in grey, orange, and blue, respectively. Coordinates for replicate measurements on

905 the same line were averaged. RC line is shown in black. Error bars represent the standard
906 deviation.
907
908 Figure S14. PCA of NPQ relaxation in the NAM population on 8/20/22. Diverse, elite, and PI
909 lines are shown in grey, orange, and blue, respectively. Coordinates for replicate measurements
910 on the same line were averaged. RC line is shown in black. Error bars represent the standard
911 deviation.
912
913 Figure S15. PCA displaying the relationships between the NPQ relaxation parameters and the
914 environment in (a-d) 2021 (1296 observations) and (e-h) 2022 (1025 observations). (a, c, e, and
915 g) PCA showing the spatial distribution of the different observations on the principal components
916 (PC). The circular shapes represent observations, with different colors representing different
917 days. The triangular shapes show the average of different NAM groups at different day, with
918 diverse, elite, PI, and RC groups shown in grey, orange, blue and black, respectively. For each
919 group, a solid line connect those points to represent their evolution throughout the season. (b, d,
920 f, and h) The correlation circle showing the relationships between variables. Variables related to
921 the NPQ relaxation parameters, and the environments are represented in red and black,
922 respectively. The percentage of total variance explained by the PC1, PC2, and PC3 is shown on
923 the axis title.

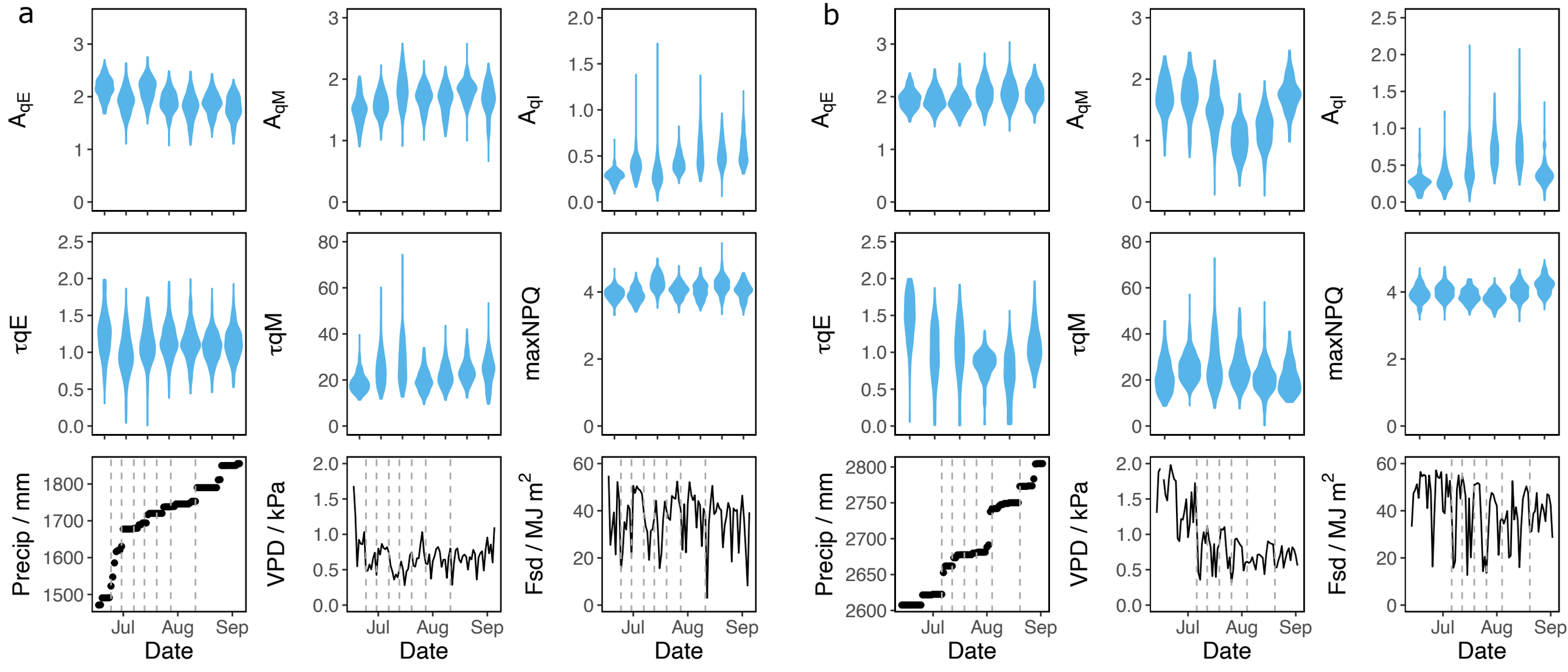
a
b
A_{qE}
A_{qM}
A_{qI}
τqE
τqM
maxNPQ
Precip / mm
VPD / kPa
Fsd / MJ m^2
Jul
Aug
Sep
Date

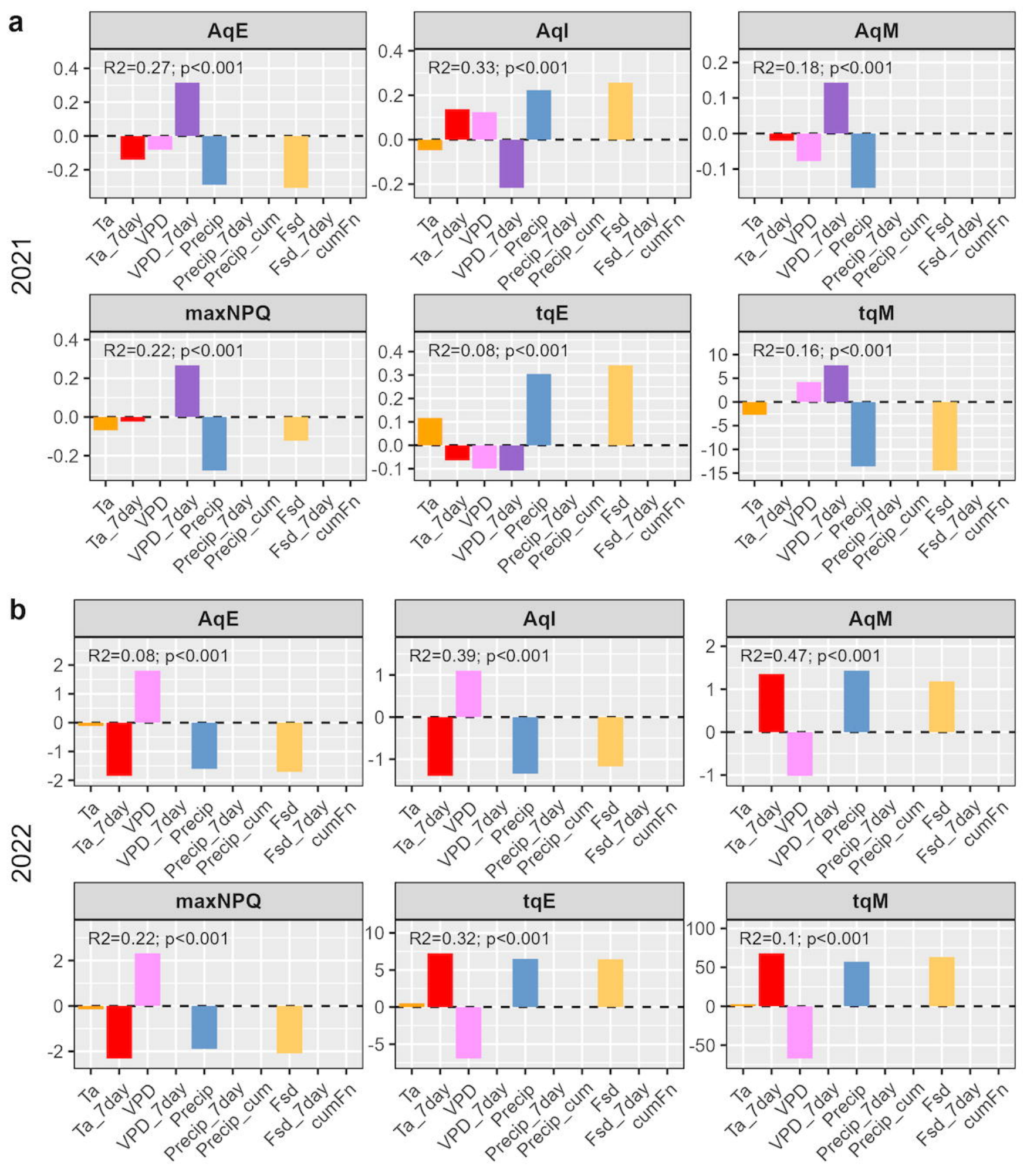
a
2021
AqE
R2=0.27; p<0.001
AqI
R2=0.33; p<0.001
AqM
R2=0.18; p<0.001
maxNPQ
R2=0.22; p<0.001
tqE
R2=0.08; p<0.001
tqM
R2=0.16; p<0.001
b
2022
AqE
R2=0.08; p<0.001
AqI
R2=0.39; p<0.001
AqM
R2=0.47; p<0.001
maxNPQ
R2=0.22; p<0.001
tqE
R2=0.32; p<0.001
tqM
R2=0.1; p<0.001
Ta
Ta_7day
VPD
VPD_7day
Precip
Precip_7day
Precip_cum
Fsd
Fsd_7day
cumFn

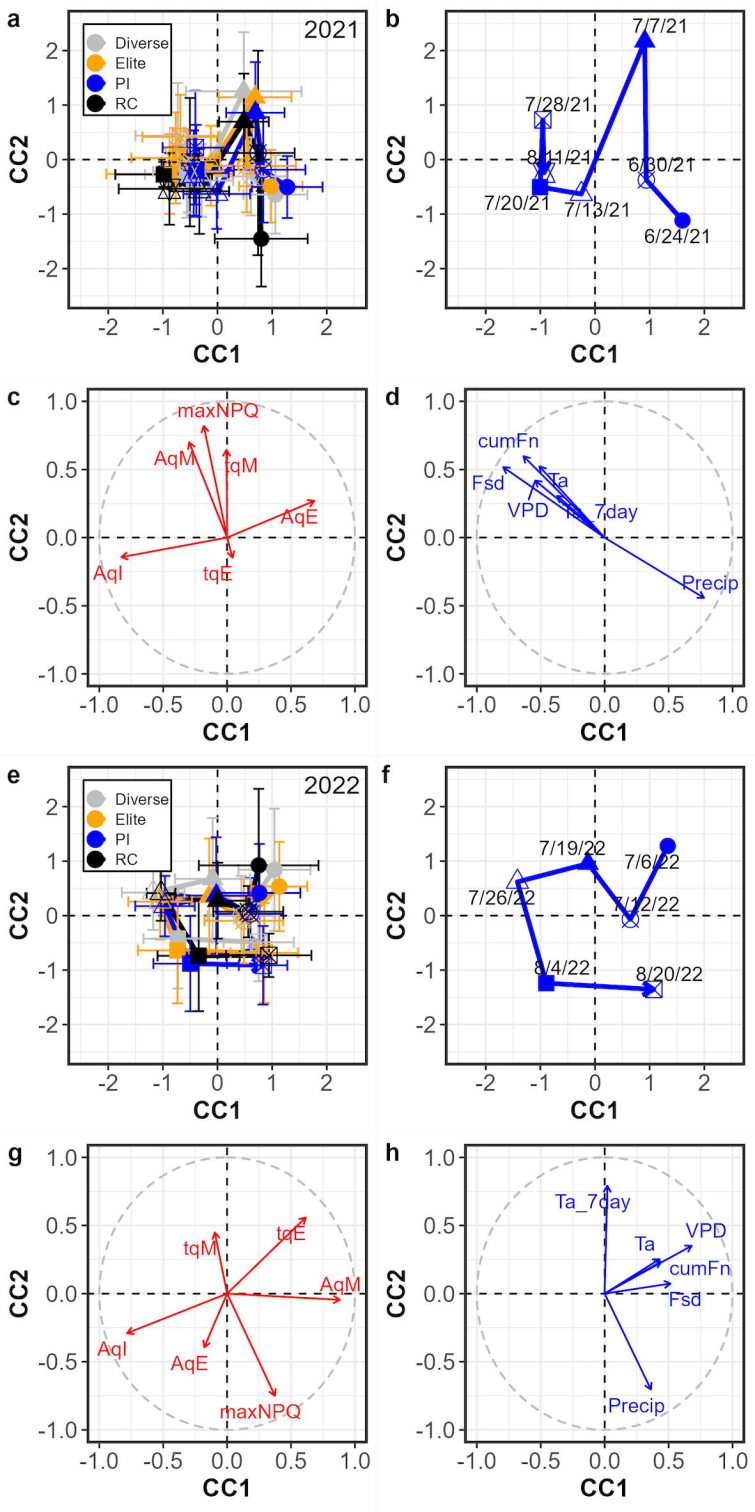
a
2021
Diverse
Elite
PI
RC
CC1
CC2
b
7/7/21
7/28/21
8/11/21
6/30/21
7/20/21
7/13/21
6/24/21
c
maxNPQ
AqM
tqM
AqE
AqI
tqE
d
cumFn
Fsd
Ta
VPD
Ts
7day
Precip
e
2022
f
7/19/22
7/6/22
7/26/22
7/12/22
8/4/22
8/20/22
g
tqM
tqE
AqM
AqI
AqE
maxNPQ
h
Ta_7day
VPD
Ta
cumFn
Fsd
Precip

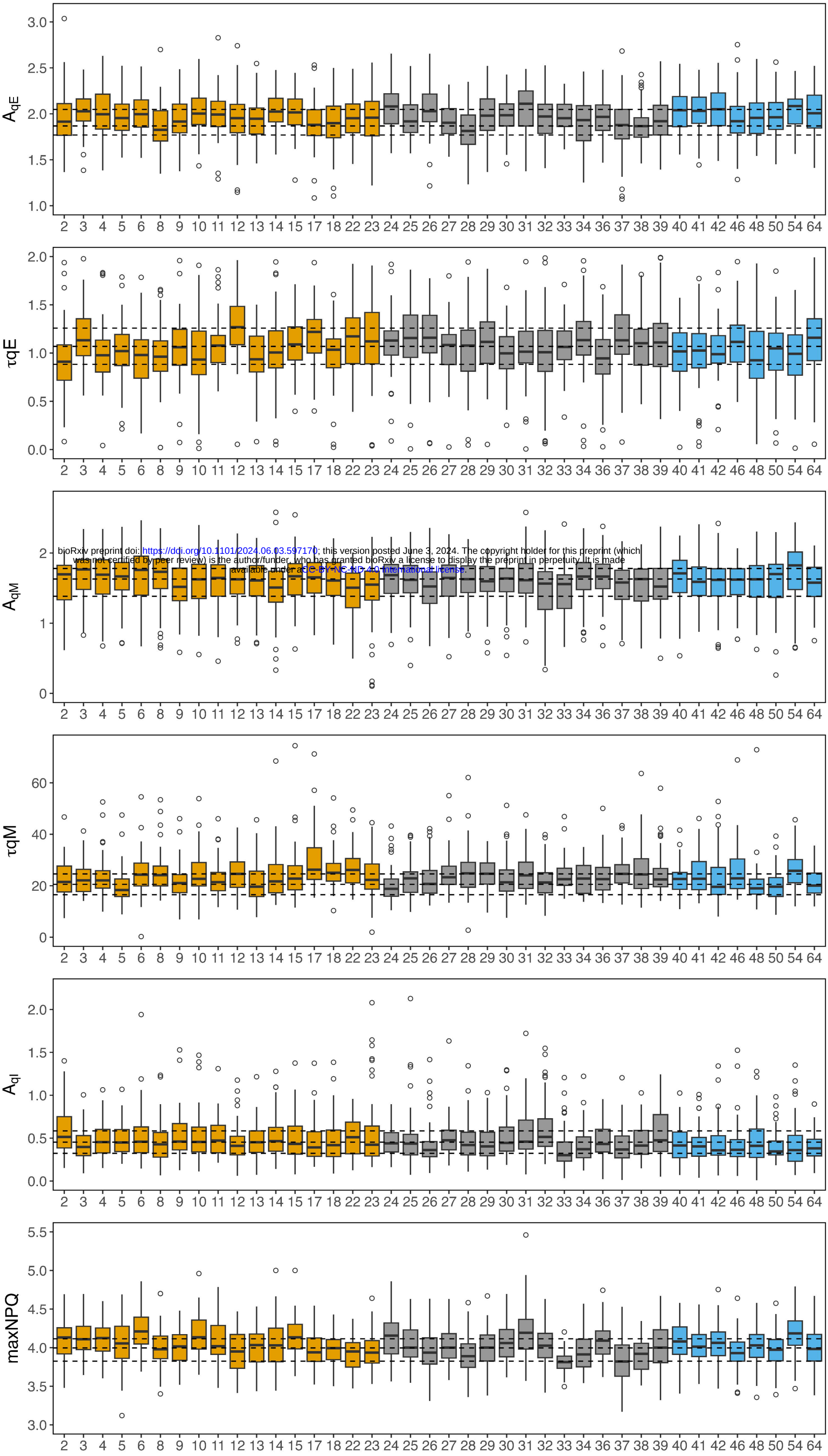

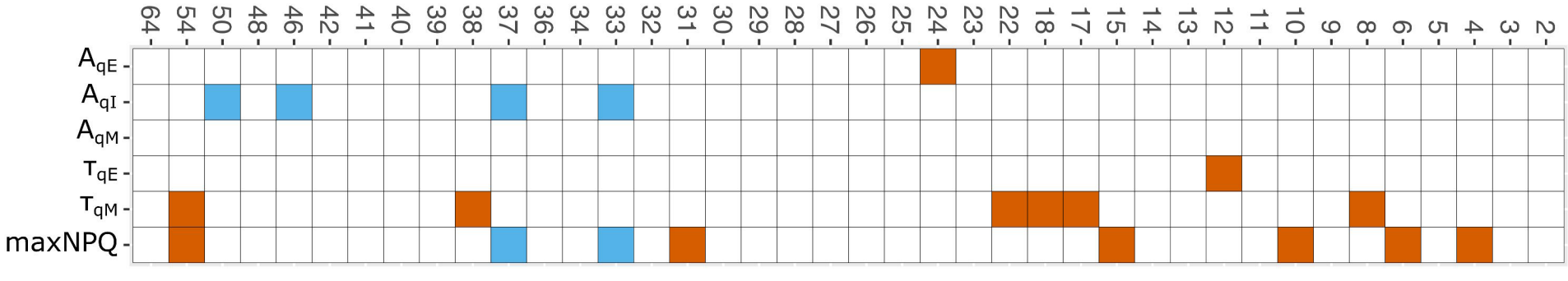
64
54
50
48
46
42
41
40
39
38
37
36
34
33
32
31
30
29
28
27
26
25
24
23
22
18
17
15
14
13
12
11
10
9
8
6
5
4
3
2
AqE
AqI
AqM
TqE
TqM
maxNPQ

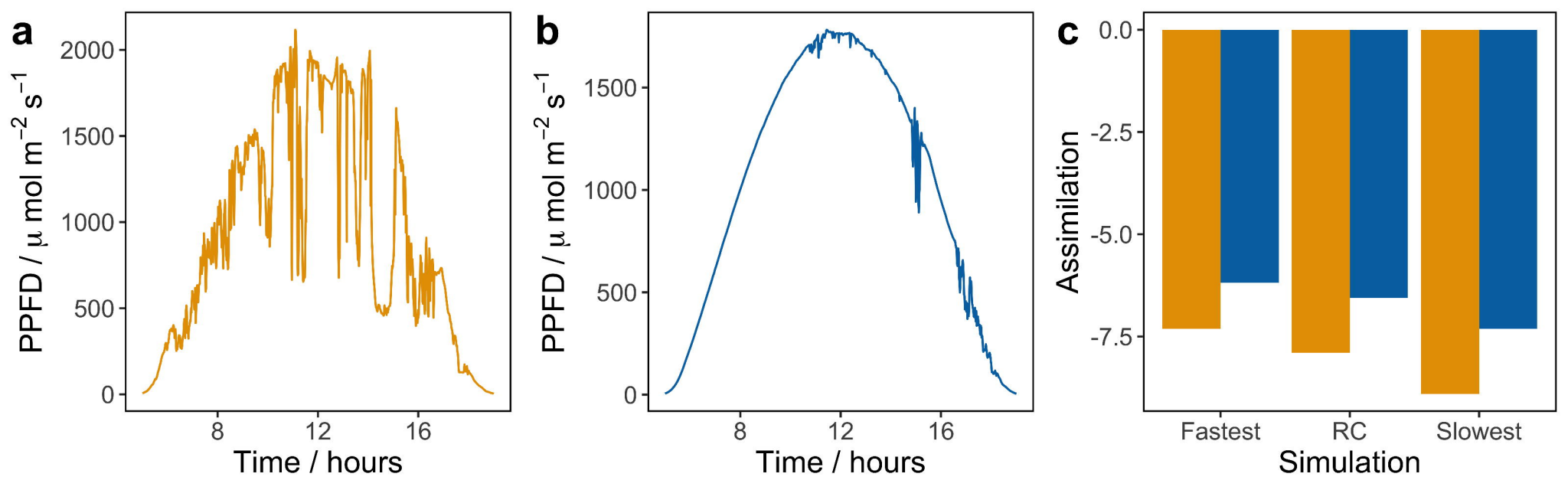
a
b
c
PPFD / μ mol m^{-2} s^{-1}
2000
1500
1000
500
0
8
12
16
Time / hours
Assimilation
0.0
-2.5
-5.0
-7.5
Fastest
RC
Slowest
Simulation